JOURNAL OF MODERN OPTICS, 2003, VOL. 50, NO. 10, 1509–1520

Detection of nanoparticles using optical gradient forces

FILIPP V. IGNATOVICH, ACHIM HARTSCHUH and LUKAS NOVOTNY

The Institute of Optics, University of Rochester, Rochester, NY, 14627; e-mail: novotny@optics.rochester.edu

(*Received 5 June 2002; revision received 9 September 2002*)

Abstract. We present a detection scheme for nanoscale particles based on the gradient force and torque near a tightly focused laser beam. The focus affects the path of nanoparticles passing by and a quadrant detector records the particle trajectory. A feedback system continuously adjusts the laser power and thereby prevents the particles from being trapped. Particle size and shape can be assessed by evaluating the time-trace of the quadrant detector signal.

1. Introduction

The ability to detect nanoscale particles is important for applications such as biosensors, contamination/emission control, remote sensing and many others. The development and evaluation of particle measurement methods is one of the highest research priorities of the Environmental Protection Agency (EPA) [1]. There is increasing concern regarding the potential health effects associated with inhalation of ultra-fine particles originating from emissions of various kinds. It was shown that lung deposition peaks at 60% for 0.03 μm particles [2]. These high deposition levels in the upper respiratory system may aggravate symptoms of rhinitis and allergies and are associated with other morbidity and mortality. Various optical techniques are currently used by EPA for continuous particle sampling [3]. These rely exclusively on light scattering or light absorption. Examples are the nephelometer [4] and the optical particle counter (OPC) [5, 6]. Light scattering measurements are very sensitive to small changes in particle size but they are often aimed at measuring collections of particles. The signal is averaged over an ensemble of particles and it is assumed that there is no variation in the size distribution within the sampling time. The signal-to-noise ratio is limited by the large sampling volume. The minimum detectable particle size is reported to be $\approx 0.2\,\mu$m. This limit can be overcome with condensation nuclei counters (CNC) which sense ultra-fine particles by causing them to grow to a size that is efficiently detected by light scattering [7]. However, CNCs are not as accurate as other methods owing to the upper limit of the particle size.

Particles can also be classified based on their scattering pattern (pattern recognition). However, in order to generate a pattern different from a dipole radiation pattern, higher multipole orders have to become significant. This is only the case for particles larger than the size of the wavelength. For example, the quadrupole scattering cross-section for a $\approx 0.25\,\mu$m polymer particle in water and

Journal of Modern Optics ISSN 0950–0340 print/ISSN 1362–3044 online
http://www.tandf.co.uk/journals
DOI: 10.1080/0950034031000064924

irradiated at $\lambda = 800\,\text{nm}$ is more than a factor of 10 lower than the corresponding dipole scattering cross-section [8].

In biomedical applications it is important to be able to measure physical and/or chemical characteristics of cells and other biological particles. Flow cytometry is a technique in which such measurements are made while the cells or particles pass through the measuring apparatus in a fluid stream. Flow sorting extends flow cytometry by using electrical or mechanical means to divert and collect cells with particular measured characteristics. Most of the developed and even commercialized techniques for flow cytometry [9–11], are based on the reverse scattering problem within the Mie theory framework [8]. As a result, these methods do not work for particles much smaller than the wavelength. Although these methods were discussed theoretically for particles down to 0.1 μm [12], measurements down to 0.5 μm only were reported [10].

The detection of biological warfare agents is also one of the top priorities of the Department of Defence. In particular making a detector able to determine the presence of rogue viruses in the field conditions is a challenging task, as the smallest virus used in the bio-warfare, Flavivirus, has a diameter of 45 nm [13].

Optical methods for the detection and classification of nanoscale particles seem to be favourable for reasons of fastness, simple implementation and low maintainance. Challenges are the inverse scattering problem and the low sensitivity for very small particles. In general, the scattering efficiency of subwavelength-sized particles scales with the square of the particle polarizability α_p and hence with R^6, with R being the particle radius. Because of signal-to-noise limitations, this strong size dependence prevents the detection of very small particles. On the other hand, the gradient force [14, 15] acting on particle scales only linearly with α_p and thus with R^3. It is therefore intuitive to use gradient force for the detection of subwavelength-sized particles.

2. Principle of the gradient force detecor

We developed a method which can recognize nanoparticles in the size range of typical biowarfare viruses by detecting the optical force exerted on the nanoparticle by a tightly focused laser beam. A quadrant detector is used to detect the light scattered from a nanoparticle passing by a tightly focused laser beam (figure 1). An electro-optical modulator controls the laser intensity before the beam is focused into a flow cell. A particle will be accelerated or deflected from its original path when it travels near or through the laser focus. The scattered light from the particle is detected by a quadrant detector which collects the transmitted light through the flow cell. This signal allows us to monitor the particle's trajectory and its deflection from the original path. Another detector located in reflection is used to extend the sensor's detection range. A high laser intensity is required to sense small particles. However, high intensities trap big particles and hence block the sensor. In order to prevent this scenario, the detector in reflection is integrated into a feedback loop. When a particle passes through the focus, the detector registers the light reflected from the particle and the feedback controller automatically attenuates the laser intensity to prevent trapping.

The idea of using a quadrant detector to monitor the motility of a bead in the focus of a microscope objective was first introduced by Gittes *et al*. [16]. The authors in this work developed a technique by which lateral position of an optically

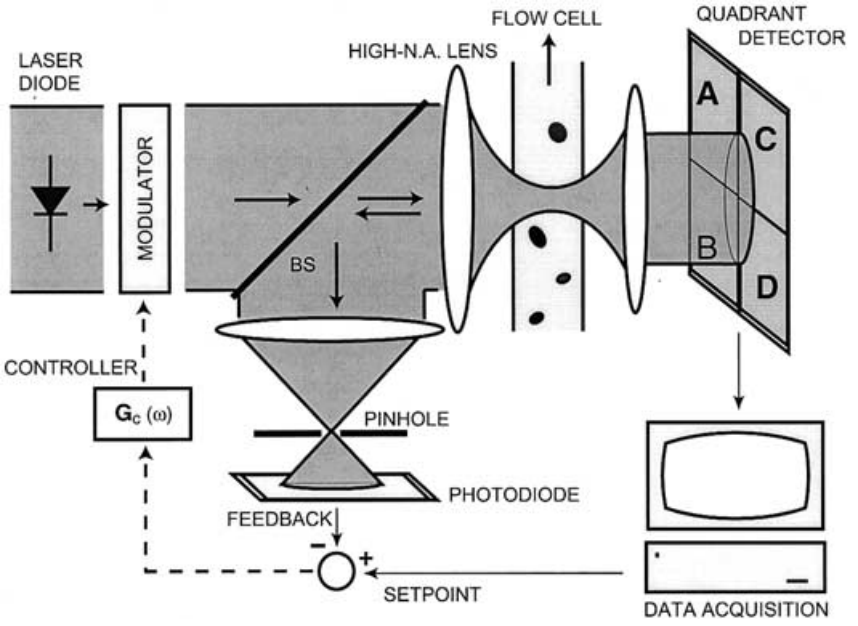

Figure 1. Illustration of the gradient-force nanoparticle detector. Light from a laser source is tightly focused into a flow cell. Particles moving in the flow cell are deflected from their original path due to the optical gradient force. The deflection is monitored by a quadrant detector located in transmission. A detector located in reflection is integrated into a feedback loop which prevents particles from being trapped by automatically attenuating the laser intensity.

trapped object in a microscope can be monitored by measuring the intensity shifts in the back focal plane of the lens that collimates the outgoing laser field. The detected intensity shift originates from interference between the original laser field and the scattered field from the particle. The signal depends on the relative position of the particle with respect to the focus.

Defining the signal from each quadrant by A, B, C and D (figure 2), motion in the x-direction will induce a change in the signal $(A+C)-(B+D)$. On the other hand, motion in the y-direction can be detected by monitoring the signal $(A+B)-(C+D)$. The two signals can be made independent of the laser intensity by normalization with signal $A+B+C+D$.

3. Theoretical considerations

In order to understand the process of position tracking, let us calculate the scattered field at the position of the detector. Assume that the focus is located at the origin and the particle is located at the point $\mathbf{r_0} = \{x_0, y_0, z_0\}$. The particle radius is R and the field incident on the particle is $\mathbf{E}(\mathbf{r_0})$. The incident beam is a paraxial Gaussian TEM_{00} mode polarized in the x-direction ($\mathbf{E} = E\mathbf{n}_x$) and propagating along the z-direction. The centre of the detector is located at the point $(0, 0, z)$ (c.f. figure 3). Since we consider particles much smaller than the laser wavelength we treat the particles in the dipole (Rayleigh) limit. The polarizability of a particle reads

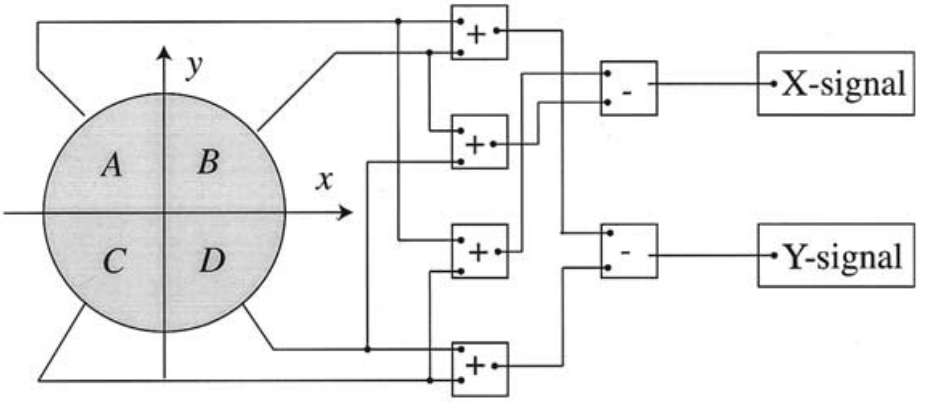

Figure 2. Computation of the differential signals Δx and Δy given the signals from the quadrant detector. The differential signal Δx represents a particle's motion along the flow channel (x-direction). The differential signal Δy represents a particle's motion transverse to the flow channel (y-direction).

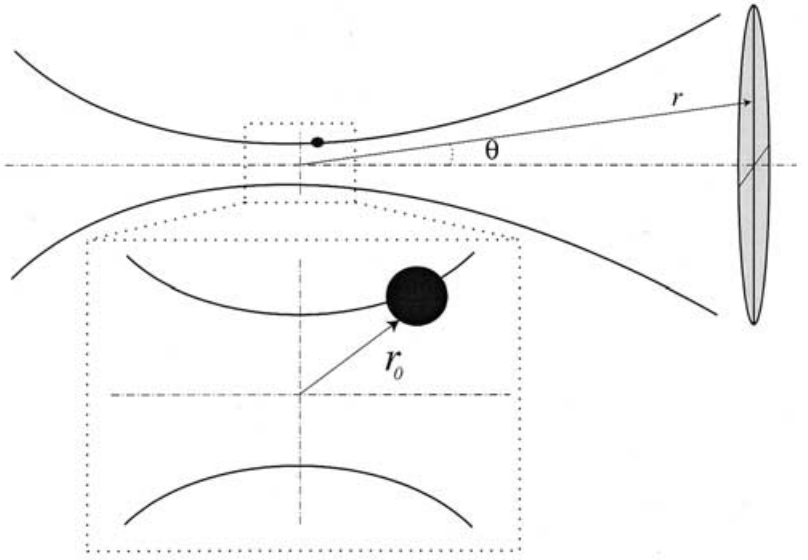

Figure 3. Illustration of the relative position of the detector and a particle near the laser focus. The parameters indicated in the figure are used in the derivation of equations (10)–(11). Because of the large distance between particle and detector the angle θ is approximately the same for all particle positions near the laser focus.

$$\alpha_p(\omega) = 3\varepsilon_0\varepsilon_s \frac{4\pi R^3}{3} \frac{\varepsilon_p - \varepsilon_s}{\varepsilon_p + 2\varepsilon_s}, \tag{1}$$

where ε_p is the particle's dielectric constant and ε_s is the dielectric constant of the surrounding medium [8]. The field scattered by the particle is calculated in the far-zone as

$$\mathbf{E}_p(\mathbf{r}) = \frac{\omega^2}{c^2}\frac{1}{\varepsilon_0}\overleftrightarrow{\mathbf{G}}_{ff}(\mathbf{r},\mathbf{r_0})\mathbf{p}, \tag{2}$$

where $\overleftrightarrow{\mathbf{G}}_{ff}$ is the far-field part of the dyadic Green's function and the dipole moment $\mathbf{p}$ is linearly related to the incident laser field as $\mathbf{p} = \alpha_p \mathbf{E}(\mathbf{r}_0)$. Using the explicit expression for $\overleftrightarrow{\mathbf{G}}_{ff}$ we obtain

$$\mathbf{E}_p(\mathbf{r}) = \frac{\pi\alpha_p}{\varepsilon_0\lambda^2 z}|E(\mathbf{r}_0)|\left(1 - \frac{(\mathbf{r}\cdot\mathbf{n}_x)^2}{r^2}\right)\mathrm{e}^{i[\phi_0 + kr(1-\mathbf{r}\cdot\mathbf{r}_0/r^2)]}\mathbf{n}_x, \tag{3}$$

where $\phi_0 = \arg[E(\mathbf{r}_0)]$ and $\mathbf{n}_x$ is the unit vector in x-direction.

We assume that the scattered field is much weaker than the incident field which allows us to ignore attenuation of the incident beam. As the detector is located far from the focus, the Gaussian beam can be represented as

$$\mathbf{E}(\mathbf{r}) \approx -\mathrm{i}E_0\frac{\pi w_0^2}{\lambda z}\mathrm{e}^{ikz(1+\theta^2/2) - k^2 w_0^2\theta^2/4}\mathbf{n}_x, \tag{4}$$

where we used $1/r \approx 1/z$. At the detector, the scattered field from the particle interferes with the direct field of the laser beam. The resulting intensity distribution at the detector is

$$I = |E|^2 + |E_p|^2 + 2\mathrm{Re}(E^* E_p). \tag{5}$$

The differential signal from this detector is calculated as

$$\Delta = \frac{\int_{D_+} I\mathrm{d}A - \int_{D_-} I\mathrm{d}A}{\int_D I\mathrm{d}A} \approx \frac{\int_{D_+}\delta I\mathrm{d}A - \int_{D_-}\delta I\mathrm{d}A}{\int_{waist}|E(z=0)|^2\mathrm{d}A}, \tag{6}$$

where D_+ and D_- indicate two different halves of the detector, $\mathrm{d}A$ is a differential surface area, and $\delta I = 2\mathrm{Re}(E_x^* E_{px})$.[1] The value in the denominator corresponds to the total power striking the detector which is approximately equal to the power in the beam waist. Using equations (4) and (3) in (6) we obtain

$$\Delta = \frac{\pi\alpha_p}{2\varepsilon_0\lambda^3}\left[\int_{\Omega_+} F(\theta,\phi)\mathrm{d}\Omega - \int_{\Omega_-} F(\theta,\phi)\mathrm{d}\Omega\right] \tag{7}$$

$$F(\theta,\phi) = \mathrm{e}^{-\frac{k^2 w_0^2\theta^2}{4}}\sin[kx_0\cos\phi\sin\theta + ky_0\sin\phi\sin\theta + kz_0\cos\theta].$$

The above expression for $F(\theta,\phi)$ can be simplified by expanding the sine function in terms of Bessel functions using [20]

$$\mathrm{e}^{\mathrm{i}a\cos b} = J_0(a) + 2\sum_{k=1}^{\infty}\mathrm{i}^k J_k(a)\cos(kb). \tag{8}$$

Keeping only the two lowest order terms we obtain

$$F(\theta,\phi) = \mathrm{Im}[\mathrm{e}^{ikz_0\cos\theta}\{J_0(k\rho_0\sin\theta) + 2\mathrm{i}J_1(k\rho_0\sin\theta)\cos(\phi-\phi_0)\}], \tag{9}$$

[1] Since the detector records an interference between *fields*, the signal turns out to be proportional to R^3. If the scattered intensity was recorded the signal would turn out to be proportional to R^6. The dependence on R^3 is beneficial for the detection of very small particles since it leads to a better signal-to-noise ratio than the R^6 dependence inherent to non-interferometric scattering.

where $x_0 = \rho_0 \cos\phi_0$ and $y_0 = \rho_0 \sin\phi_0$. Now we are able to carry out the analytical integration over ϕ in equation (7). We obtain two signals Δx and Δy. For Δx, Ω_+ and Ω_- designate the upper and lower halves of the detector, respectively, and for Δy they denote the right and left halves of the detector, respectively. The resulting expressions are

$$\Delta x = \frac{\pi\alpha_p}{2\varepsilon_0\lambda^3}\sin(\arctan[y_0/x_0]) \int_0^{\theta_{\max}} \mathrm{e}^{-k^2 w_0^2\theta^2/4} \cos(kz_0\cos\theta) J_1(k\sqrt{x_0^2+y_0^2}\sin\theta)\theta \mathrm{d}\theta \tag{10}$$

$$\Delta y = \frac{\pi\alpha_p}{2\varepsilon_0\lambda^3}\cos(\arctan[y_0/x_0]) \int_0^{\theta_{\max}} \mathrm{e}^{-k^2 w_0^2\theta^2/4} \cos(kz_0\cos\theta) J_1(k\sqrt{x_0^2+y_0^2}\sin\theta)\theta \mathrm{d}\theta, \tag{11}$$

where $\theta_{\max}$ is equal to one half of the angular aperture of the collimating objective. These equations are very convenient for numerical calculations, as they require much less computer time than the evaluation of the double integral in equation (7).

3.1. *Numerical calculations*

The equation of motion for a polarizable particle with mass m moving in a viscous medium (viscosity η) with velocity v and experiencing the gradient force exerted by the laser focus is calculated as

$$m\ddot{\mathbf{r}}_0 = 6\pi\eta R(\dot{\mathbf{r}}_0 - \mathbf{v}_0) + \frac{\alpha_p}{2}\nabla|\mathbf{E}(\mathbf{r}_0)|^2, \tag{12}$$

where m is particle mass, $\mathbf{v_0}$ is the speed of the liquid, α_p is particle polarizability and $\mathbf{E}(\mathbf{r}_0)$ is the electric field at the location of the particle. The first term on the right-hand side is the Stokes force due to viscous drag; the viscosity of water, η, is $10^{-3}\mathrm{Nsm}^{-2}$ at $300^\circ F$. In principle, a random force has to be included in order to account for the fluctuating environment (Brownian motion). However, as a first step we assume that the random force is much weaker than the Stokes force and the trapping force which allows us to ignore it. The particle's trajectory is defined by an initial position and velocity. We used the Runge–Kutta method to numerically study different particle trajectories. The initial laser power is chosen to be 100 mW. The feedback loop, defined by its transfer function, has also been implemented in the numerical scheme. It automatically attenuates the laser power by an amount which depends on the strength of the backscattered intensity.[2] The particles are moving with a water flow at $30\,\mu\mathrm{m\ s}^{-1}$ in the x-direction. The numerical aperture of the focusing objective is $NA = 1.3$ and the wavelength is $\lambda = 830\,\mathrm{nm}$ (the focal spot is $w_0 \approx 0.61\lambda/NA \approx 400\,\mathrm{nm}$). The particles are incident from an infinite distance ($x_0 \to -\infty$). We consider two cases: (1) a particle passing exactly through the laser focus ($y_0 = 0$, $z_0 = 0$) and (2) a particle which is displaced from the straight trajectory through the laser focus ($y_0 = 0.5\,\mu\mathrm{m}$, $z_0 = 0$).

[2] We introduced two parameters; one describes the back reflection from the particle and the other denotes the background noise level (scattering from solution and interfaces). Both parameters depend on the laser power. The laser intensity is adjusted such that the background noise level plus reflected light intensity equal to a constant.

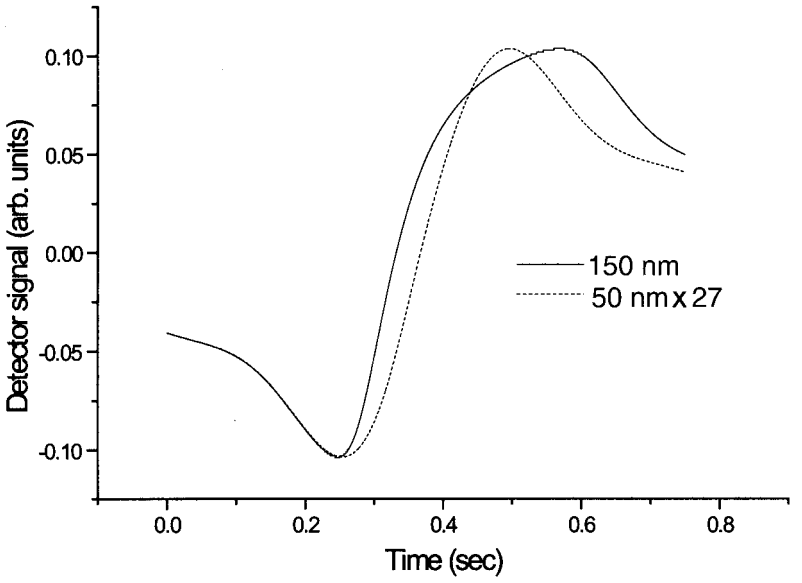

Figure 4. Calculated quadrant detector signal (Δx) for a 50 nm and a 150 nm particle passing exactly through the laser focus. The two particles can be clearly distinguished based on the different time traces. Note that the time trace for the 50 nm particle is scaled by a factor of 27 in the amplitude. See text for details.

Figure 4 shows the calculated Δx-signal for case 1) and for the two particle sizes $2R = 50$ nm and $2R = 150$ nm. The initial conditions are the same for both particles. The Δy-signal is zero for all times since the particle travels along the x-axis. Note that the time trace for the 50 nm particle is scaled by a factor of 27 in the amplitude. The feedback loop attenuates the laser intensity as the particles approach the laser focus (figure 5). Using the parameters of the numerical experiment, the drag force at $30\,\mu\mathrm{m\,s^{-1}}$ for 150 nm particle is ≈ 0.04 pN. The maximum gradient force it experiences is ≈ 0.4 pN, thus it may be trapped if the feedback loop is open. The drag force for 50 nm at $30\,\mu\mathrm{m\,s^{-1}}$ is ≈ 0.02 pN, and the maximum gradient force is ≈ 0.01 pN. We chose our parameters this way in order to demonstrate the importance of the feedback loop for preventing particles from being trapped. The following difference between the two curves in figure 4 can be recognized: the 150 nm particle is initially accelerated towards the laser focus but due to the Stokes force it slows down at the centre of the beam because the net elastic restoring force provided by the optical field gradient approaches zero. As it is carried away by the fluid the feedback increases the laser intensity and pulls the particle back.[3] Consequently, the time-trace for the 150 nm particle appears to be

[3] Particle motion in a liquid is so overdamped that one may neglect completely the interial term in equation (12), giving

$$6\pi\eta R(\mathbf{v}_0 - \dot{\mathbf{r}}_0) = \frac{\alpha_p}{2}\nabla|\mathbf{E}(\mathbf{r}_0)|^2.$$

This means that the particle's velocity at every point is determined by the gradient force. When the particle approaches the focus, the particle acquires velocity relative to the water. Before passing through the focus it moves faster than the liquid and after passing the focus it moves slower.

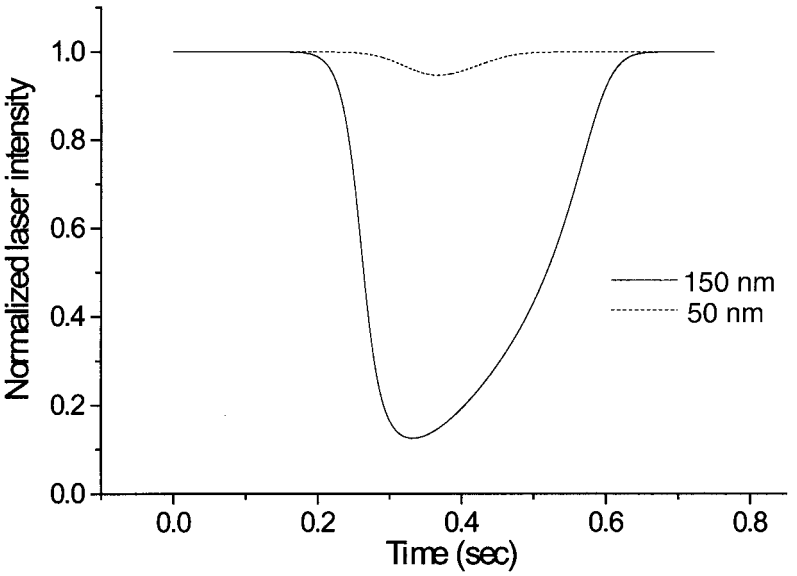

Figure 5. Calculated laser intensity for a 50 nm and a 150 nm particle passing exactly through the laser focus. The feedback loop automatically attenuates the laser intensity in order to prevent trapping of the larger particle.

wider than the time trace for the 50 nm particle. Also, the two time traces show different asymmetries: for the 150 nm particle the first half of the trace is steeper than for the 50 nm particle, and the opposite situation applies for the second half of the curve.

The picture changes marginally if the particles do not pass exactly through the laser focus but at some distance from it (case 2). In this situation, the bigger particle experiences stronger deflection from its original path than the smaller particle (figure 6(*a*)). Figure 6(*b*) contains two graphs for this case. The first graph is the Δx-signal representing the motion along the x-axis. The second graph is the Δy-signal which reflects the motion along the y-axis, i.e. transverse to the flow cell. The main difference from case (1) is that the y-signal is not zero. Furthermore, although the width of the Δx-signal for the 150 nm particle is larger than for the 50 nm particle, the width of the Δy-signal turns out to be less. This is caused by the fact that the 150 nm particle is pulled faster towards the focus and therefore traverses the $x = 0$ line (maximum of the Δy-signal) faster than the 50 nm particle.

The following parameters can be extracted from the Δx and Δy curves of a certain particle: amplitude, width and slope. This makes a total of six parameters for the two curves. On the other hand, there are four unknown parameters in the experiment: (1) smallest distance to the focus in y-direction ($y_{\min}$); (2) smallest distance to the focus in the z-direction ($z_{\min}$); (3) the particle size R; and (4) the particle refractive index n. Thus, in principle, it is possible to distinguish between the particles if the mapping can be made mathematically unique. The solution to this inverse problem demands the implementation of an intelligent evaluation algorithm.

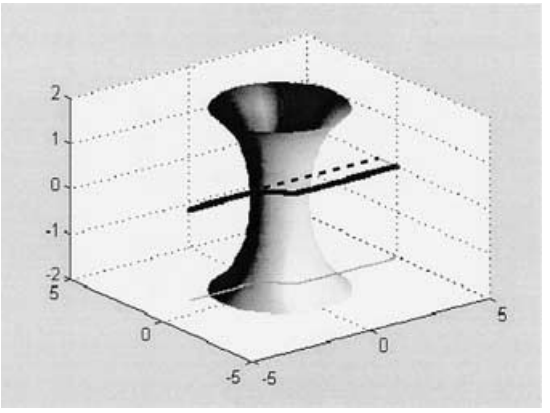

(*a*)

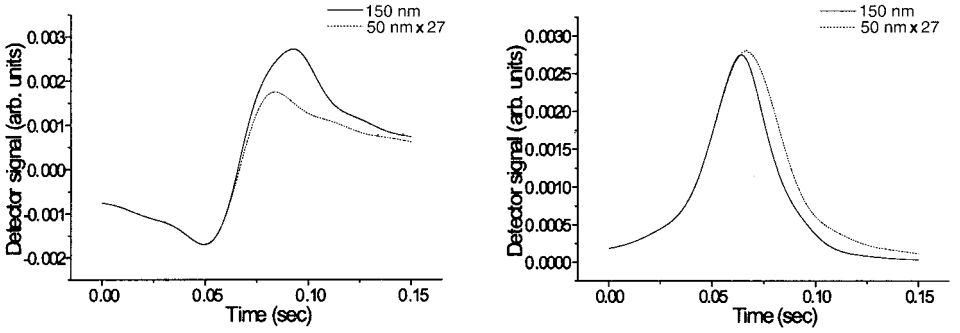

(*b*)

Figure 6. Calculated quadrant detector signals (Δx and Δy) for a 50 nm and a 150 nm particle not passing exactly through the laser focus. Δx (left graph) and Δy (right graph). See text for details.

So far, our discussion has focused on spherical particles, however, the outlined scheme is very well suited to the detection of ellipsoidal particles because of the torque exerted by the laser focus on non-spherical particles. The torque can be well incorporated into the equation of motion (12). In the experimental situation, ellipsoidal particles move in random orientations towards the laser focus. The latter forces the particles to align in a certain direction depending on the momentary position of the particle [17]. A change in orientation will result in a change of the scattered field which will be seen as a modulation of the Δx and Δy signals. The modulation frequency therefore provides information about eccentricity of the particles.

4. Experimental considerations

The measurement of small particles, even in the interferometric scheme presented here, is a challenging task. First, the laser source needs to be very stable, with no mode hopping and with the highest possible pointing stability. Mode hopping gives rise to changes in the interference pattern thereby affecting the differential signals (Δx and Δy). Unfortunately, for single-mode semiconduc-

tor lasers it is very difficult to avoid this problem. Even if the laser is optically isolated from back reflections of consequential optical elements, back reflections from the optical isolator itself still lead to mode hopping problems at high power levels (>100 mW). The pointing instability causes the laser focus to drift around, thus causing errors in measurements of the position of a particle. To reduce this problem Gittes *et al.* implemented a feedback controlled pointing stabilizer [16]. Also, laboratory air movements add to the pointing instability, especially for longer beam paths. With the use of plastic guide tubes the laser beam can be shielded from air movement and from dust particles traversing the laser beam.

Before being operational, the system needs to be calibrated. Polystyrene beads are commonly used as calibration particles because of their uniform size distribution. The index of refraction of polystyrene spheres is very well known ($n = 1.59$). Dielectric constants of biological matter have very similar optical properties, for example, $n = 1.51$ for a protein, $n = 1.48$ for lipids, and $n = 1.42$ for mitochondria. The particles can be introduced into either a liquid or a gas. Water is very convenient to use in a laboratory due to its optical properties and high viscosity coefficient. Air is a more desirable choice in a simple device to perform virus monitoring in the field, however, it possesses a number of disadvantages. The Brownian motion in the air is greater than in the water. Also, the reflection from the objective/air interface, is much stronger than from the objective/liquid interface which reduces the sensitivity of the reflective detection part. The effective gradient force will be reduced when focusing in air because of the stronger index mismatch between the walls of the microfluidic channel and the enclosed medium. The NA can only be maintained in the vicinity of the walls but at larger distances the focus will be distorted and the NA reduced. The Brownian motion in air can be reduced using a high speed focused air jet. However, a focused air jet relies on a high particle velocity which requires large detection bandwidth. This compensates the signal-to-noise advantage due to smaller fluctuations.

Since the sensor relies on the evaluation of particle trajectories, it is important to accurately control the speed of the host medium. In order to ensure that there are no velocity gradients across the area of interest a liquid host medium is advantageous. The velocity of the liquid can be controlled by applying a voltage between electrodes placed into the liquid (electro-osmosis) [18]. Velocity control by electro-osmosis has the advantage of generating a gradient-free flow as opposed to pressure-driven velocity control. Liquids have the further advantage that they can be sent through nanoscale channels smaller in diameter than the beam waist of the laser focus [19]. With such small channels a constant intensity distribution across the flow channel can be generated thereby reducing the number of unknown parameters. The only unfavourable aspect of liquids is the technical challenge of using liquids in small, integrated devices.

Another source of noise is associated with the detection process. Because the quadrant detector is irradiated in a forward direction (transmission mode) it works in the signal-limited mode, i.e. it is dominated by shot noise. Therefore, the stronger the signal, the better the signal-to-noise ratio (SNR). The advantage of transmission mode operation is that the SNR does not depend on the detector area, which allows one to choose large detectors, simplifying alignment procedures. According to figure 4, the maximum differential signal from a 50 nm particle is on the order of 10^{-4}. To accurately detect this signal, the shot noise level should be less than 10^{-5}. Simple estimates require that at least 10^{10} photons have to strike the

detector every second. For $\lambda = 830\,\text{nm}$ this corresponds to 10 nW, much smaller than the 100 mW laser power. Therefore, shot noise is not a significant source of noise. It turns out that Johnson noise from the amplifying electronics is much more significant. This source of noise can be reduced at the expense of the response time of the system by reducing the detection bandwidth. Notice that fluctuations in laser power do not contribute to the noise of the system because each quadrant of the detector is affected in the same way and upon forming the differential signal the fluctuations cancel out.

Stricter requirements apply for the detector working in reflection mode (figure 1). The signal detected by this detector is background-limited, especially for small particles. Therefore, it is advisable to use the smallest detector area possible. To optimize the SNR the detector area has to be as small as the image size of the focal area. For instance, if the area of interest is 1 μm in diameter, then, using a 100× objective, the detector size should be no more than 100 μm. A small detector in reflection mode also serves to reduce the light reflected from interfaces thereby increasing the sensitivity for small particles. A reduction of detector size can easily be accomplished by using a confocal pinhole in front of the detector.

The calculated asymmetry in the time traces has been verified experimentally. Figure 7 shows the experimentally measured time traces for a 500 nm particle and a 100 nm particle. As expected, the curve for the 500 nm particle is asymmetric whereas the curve for the 100 nm particle is not. To record these curves, we used a

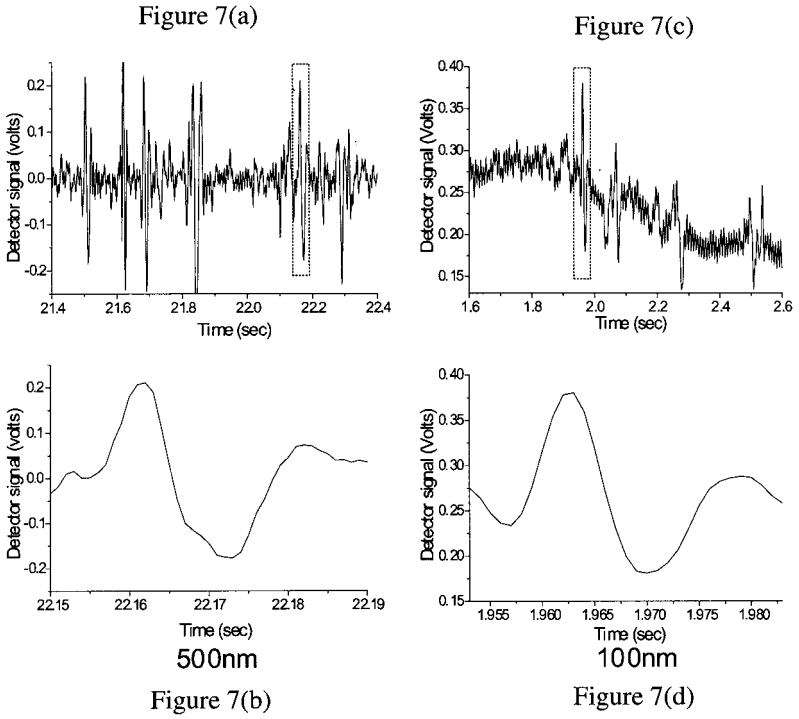

Figure 7. Experimental measurements of the quadrant detector signal for particles passing close to the focus. (*a*), (*b*) 500 nm particles trace; (*c*), (*d*) 100 nm particle trace. Dashed rectangles show magnified area. Notice asymmetry in (*b*) compared to (*d*).

$\lambda = 830\,\text{nm}$ diode laser operating at 20 mW, and a 100× objective with $NA = 1.3$. The particle solution had a speed of approximately $30\,\mu\text{m}\,\text{s}^{-1}$ and it was moved by the electro-osmotic effect.

5. Conclusions

We have introduced an optical detection scheme for nanoscale particles. The scheme relies on the optical gradient force exerted by a tightly focused laser beam. We have analysed the differential signals generated by a quadrant detector for particles with two different sizes. Experimental parameters have been discussed and it was shown that experimental realization of the particle sensor is feasible.

Acknowledgments

The authors wish to acknowledge stimulating discussions with Michael Beversluis and Alexandre Bouhelier. This work was supported by DARPA under Grant No. MDA972-00-1-0021.

References

[1] U.S. Environmental Protection Agency (1996) *Air Quality Criteria for Particulate Matter*, EPA/600/P-95/001aF-001cF (Washington, DC Office of Research and Development).
[2] Phalen, R. F. *et al.*, 1991, *Radiation Protection Dosimetry*, **38,** 179.
[3] Watson, J. G. *et al.*, 1998, Guidance for using continuous monitors in $PM_{2.5}$ monitoring networks, Office of Air Quality Planning and Standards (MD-14), US Environmental Protection Agency.
[4] Anderson, T. L., and Ogren, J. A., 1998, *Aerosol Sci. and Technol.*, **29,** 57.
[5] Fabiny, L., 1998, *Opt. Photonics News*, **9,** 34.
[6] Kerker, M., 1997, *Aerosol Sci. Technol.*, **27,** 522.
[7] Saros, M. T. *et al.*, 1996, *Aerosol Sci. Technol.*, **25,** 200.
[8] Bohren, C. F., and Huffman, D. R., 1983, *Absorption and Scattering of Light by Small Particles* (New York: Wiley).
[9] Givan, A. L., 2001 *Flow Cytometry First Principles* (New York: John Wiley & Sons).
[10] Gobel, G., Wriedt, T., and Bauckhage, K., 1998, *J. Aerosol Sci.*, **29,** 1063.
[11] Shvalov, A., Surovtsev, I. V., Chernyshev, A. V., Soini, J. T., and Maltsev, V.P., 1999, *Cytometry*, **37,** 215.
[12] Szymanski, W. W., Nagy, A., Czitrovsky, A., and Jany, P., 2002, *Measurement Sci. Technol.*, **13,** 303.
[13] Tidona, C. A., and Darai, G. (eds), 2002, *The Springer Index of Viruses* (New York: Springer)
[14] Ashkin, A., and Gordon, J. P., 1983, *Opt. Lett.*, **8,** 511.
[15] Ashkin, A., Dziedzic, J. M., Bjorkholm, J. E., and Chu, S., 1986, *Opt. Lett.*, **11,** 288.
[16] Gittes, F., and Schmidt, C. F., 1998, *Opt. Lett.*, **23,** 7.
[17] Nieminen T. A., Rubinsztein-Dunlop, H., and Heckenberg, N. R., 2001, *J. Quantitative Spectrosc. Radiative Transfer*, **70,** 627.
[18] Tsuda, T., 1995, Electro-osmosis and electrochromatography. In *Electric Field Applications in Chromatography, Industrial, and Chemical Processes*, edited by T. Tsuda (New York: Weinheim).
[19] Han, J., and Craighead, H. G., 2000, *Science*, **288,** 1026.
[20] Gradstein, I. S., and Ryzhik, I. M., 1994 *Table of Integrals, Series and Products*, equation 8.511.4 (Boston: Academic Press).